THEORETICA CHIMICA ACTA

Theoret. Chim. Acta (Berl.) 63, 421–438 (1983)


# $\pi - d$-Interaction and the Temperature Dependent Magnetic Circular Dichroism Spectra of Low Spin Fe(III)-Heme Compounds

Alexander P. Mineyev, Yurii A. Sharonov, Nataly A. Sharonova, and Yurii P. Lysov

Institute of Molecular Biology, Academy of Sciences, Moscow 117 334, U.S.S.R.

Vladimir A. Figlovsky

Institute of Bioorganic Chemistry, Academy of Sciences, Byelorusskaya SSR, Minsk, U.S.S.R.

The magnetic circular dichroism (MCD) of metmyoglobin cyanide, ferricytochrome *c* and horseradish peroxidase cyanide were measured in the region 340–800 nm over a range of temperatures from 293 to 15 K. All three species show the temperature dependent MCD (The *C*-type effects $\sim 1/T$) in both visible *Q* and near UV *B* bands. While the MCD and absorption in *B*-region as well as the absorption in *Q* region are quite similar for all three species the MCD in *Q*-bands reveal the marked differences, especially at low temperatures. To explain these observations, the theoretical treatment based on our previous model (A. P. Mineyev and Yu. A. Sharonov, 1978, Theoret. Chim. Acta (Berl.) **49**, 295–307) is proposed. The key point of this consideration is the configuration $\pi - d$-interaction which in addition to our previous analysis involves the first excited Fe(III)-ion Kramers doublet and the *B*-*Q*-mixing effects. The simultaneous least square fit of MCD and absorption data allows to evaluate the $\pi - d$-parameters which appear to be of the order of $10^2$–$10^3$ $cm^{-1}$. The role of the $\pi - d$-interaction in the forming of hemoprotein spectra are discussed.

**Key words:** Magnetic circular dichroism (MCD) – Low-spin heme compounds – $\pi - d$-interaction – Low temperatures.

Offprint requests to: A. P. Mineyev

## 1. Introduction

The techniques which are commonly used for the investigations of the electronic properties of the heme complexes may be sub-divided into two groups. The first one deals with the Fe-moiety of the heme electronic system and includes EPR spectroscopy, Mössbauer spectroscopy and magnetic susceptibility. The second group contains optical techniques which supply information mainly related to the porphyrin moiety of the heme. However because of the possible participation of porphyrin ring in some biochemical events (such as redox conversions of cytochromes), physical techniques which could detect the interaction between porphyrin and Fe-ion subsystems is worth searching for.

The low-temperature measurements of the magnetic circular dichroism (MCD) seem to be fairly effective in this sense. In the previous paper [1], the temperature dependence of MCD signals (the so called "*C*-type effects") from low-spin Fe(III)-hemoproteins has been explained in terms of exchange-type $\pi - d$-interaction. The interaction splits $\pi - \pi^*$-excited states in accordance with the mutual orientation of $\langle L_z \rangle_\pi$ and $\langle L_z \rangle_d$, which denote the expectation values of the $z$ (heme normal)-component of the orbital angular momentum operator calculated for $\pi$- and $d$-electrons, respectively.

The orbital motion is known to contribute markedly to the angular momentum of the ground Kramers doublet of low-spin Fe(III) heme complexes ($g_z \simeq 3$). When a porphyrin ring is excited in a double orbitally degenerate state the overall 4-fold (Fe+porphyrin) degeneracy will be partially lifted by $\pi - d$-interaction. Two excited Kramers doublets arise now at different energies. One of them is characterized by the parallel orientation of $\langle L_z \rangle_\pi$ and $\langle L_z \rangle_d$ and another one has the antiparallel orientation.

The external magnetic field, $H_z$, splits the ground Kramers doublet. The occupation numbers of Zeeman sublevels are governed by the Boltzmann law. Thus, on lowering the temperature the optical transitions from the lowest Zeeman sublevel will prevail. For the allowed in-porphyrin transitions a Fe-ion state must remain invariable. Therefore the fraction of the excited states with the same $\langle L_z \rangle_d$-value as that of the lowest Zeeman component of the ground state will increase as the temperature will lower. For each of the $\pi - d$-split levels there is only one state which has this $\langle L_z \rangle_d$-value. Moreover, the $\langle L_z \rangle_\pi$-values matched this $\langle L_z \rangle_d$-value are different for different $\pi - d$-levels. In the particular case these $\langle L_z \rangle_\pi$-values have the same magnitude and opposite signs. Thus the corresponding $\pi - \pi^*$-transitions are expected to be of different circular polarizations. Since they lie at different frequencies one can observe the temperature dependent MCD as shown in Fig. 1.

In paper [1] we have confined ourselves to the analysis close to what we have just described. However, neither first excited in-Fe(III)-Kramers doublet, nor $\pi - d$-mixing between $B(\pi - \pi^*)$- and $Q(\pi - \pi^*)$ states have been involved. Using such a simple model, we predicted qualitatively equivalent MCD pictures for both $B$- and $Q$-bands. Namely, the shape of an overall MCD signal was

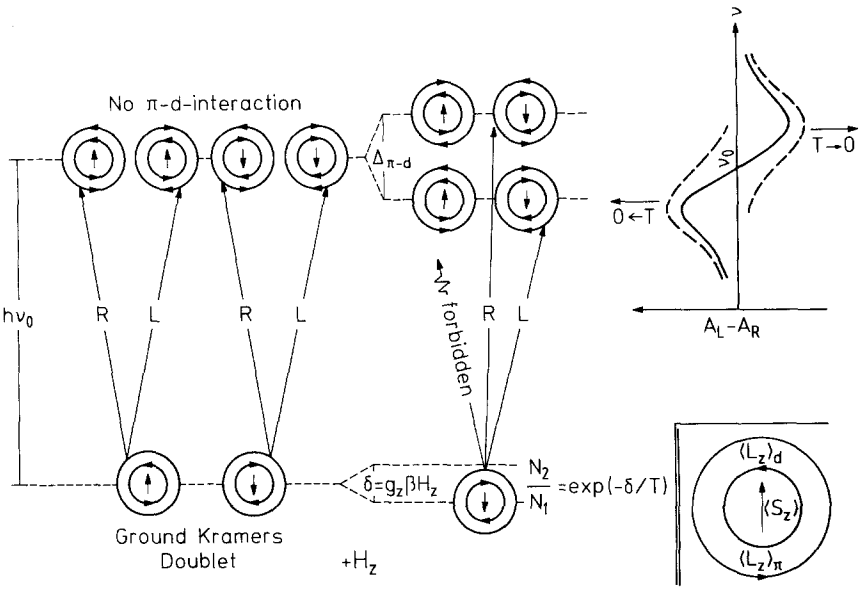


**Fig. 1.** The appearance of the *C*-type effects in the presence of $\pi-d$-interaction (see also text)

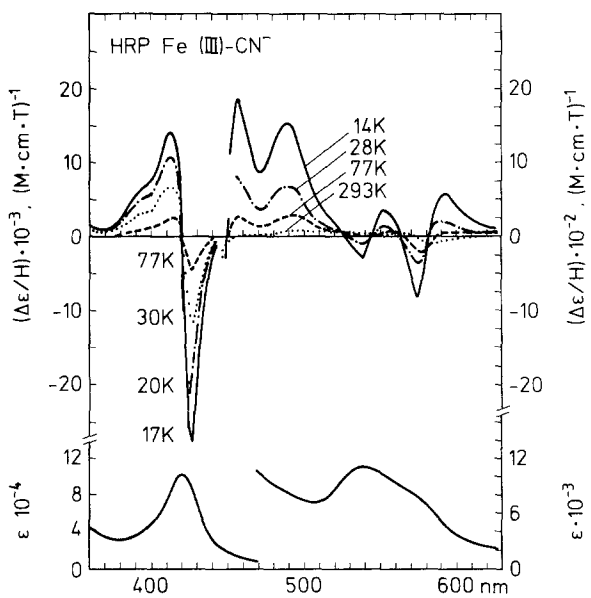


**Fig. 2.** Magnetic circular dichroism and absorption spectra of the cynanide complex of Fe(III)-horseradish peroxidase at different temperatures. Temperatures 77 K, 30 K, 20 K and 17 K in near UV and 293 K, 77 K, 28 K and 14 K in the visible. Protein concentration 1.3 $10^{-4}$ M in near UV and 3.2 $10^{-4}$ M in the visible; in 2 : 1 v/v mixture of glycerol and 0.2 M sodium phosphate buffer at pH 6.8; pathlength 1.0 mm; magnetic field 1.35 T. Absorption: room temperature

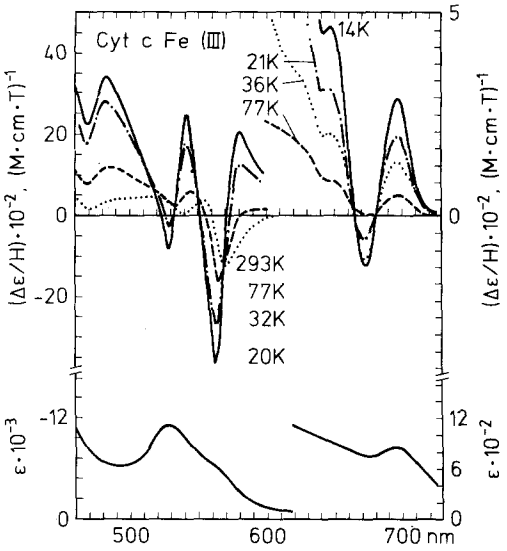


**Fig. 3.** Magnetic circular dichroism and absorption spectra of the Fe(III)-cytochrome *c* at different temperatures. Temperatures 293 K, 77 K, 32 K, 20 K in the visible and 77 K, 36 K, 21 K, 14 K in near IR. Protein concentration $1.25\,10^{-3}$ M (pathlength 1.0 mm) in the visible and $4.35\,10^{-3}$ M (pathlength 2.0 mm) in near IR; in 2:1 v/v mixture of glycerol and 0.2 M sodium phosphate buffer at pH 6.8; magnetic field 1.35 T. Absorption: room temperature

expected to be a symmetric derivative-like one in both bands. That is each band consists of two *C*-type effects of equal amplitude and opposite signs as shown in Fig. 1. The experimentally observed asymmetry of the MCD in *B*-band was not discussed in [1]. This asymmetry is naturally obtained from the improved theoretical model presented here.

The reliable evidences of the temperature dependent MCD in *Q*-band required temperatures lower than 77 K used in paper [1]. In this communication we report the MCD spectra at the temperatures down to 15 K (Figs. 2 and 3). These data provide additional experimental backgrounds for further theoretical insight into the problem.

By attemping to extend the approach reported in [1] and to explain the new experimental results, we include in our analysis both the first excited Fe(III)-ion Kramers doublet and the $\pi - d$ mixing between $B(\pi - \pi^*)$ and $Q(\pi - \pi^*)$ states.

## 2. Experimental Results

MCD spectra were recorded with an instrument constructed on a basis of a "Roussel-Jouan" dichrograph (for futher details see [2]). Low-temperature MCD measurements were performed in contact-type, germetically-closed quartz cells placed in a specially constructed cryostat. The temperature was monitored with thermocouple put into the sample.

To exclude the effects of natural CD and depolarization caused by linear birefringence in a frozen glass, the MCD spectra were obtained as a difference between the curves recorded at the opposite directions of a magnetic field.

The absorption spectra were recorded with a Beckman-26 spectro-photometer.

At the temperatures down to 15 K, we have recorded the MCD spectra of cyanide complexes of myoglobin and horseradish peroxidase as well as those of ferricytochrome *c* in the spectral region from 350 to 800 nm. Some of these MCD spectra are shown in Figs. 2–4.

Our MCD spectra of metmyoglobin cyanide agree well with liquid nitrogen and room temperature spectra published by Vickery et al. [3] but differ in intensity

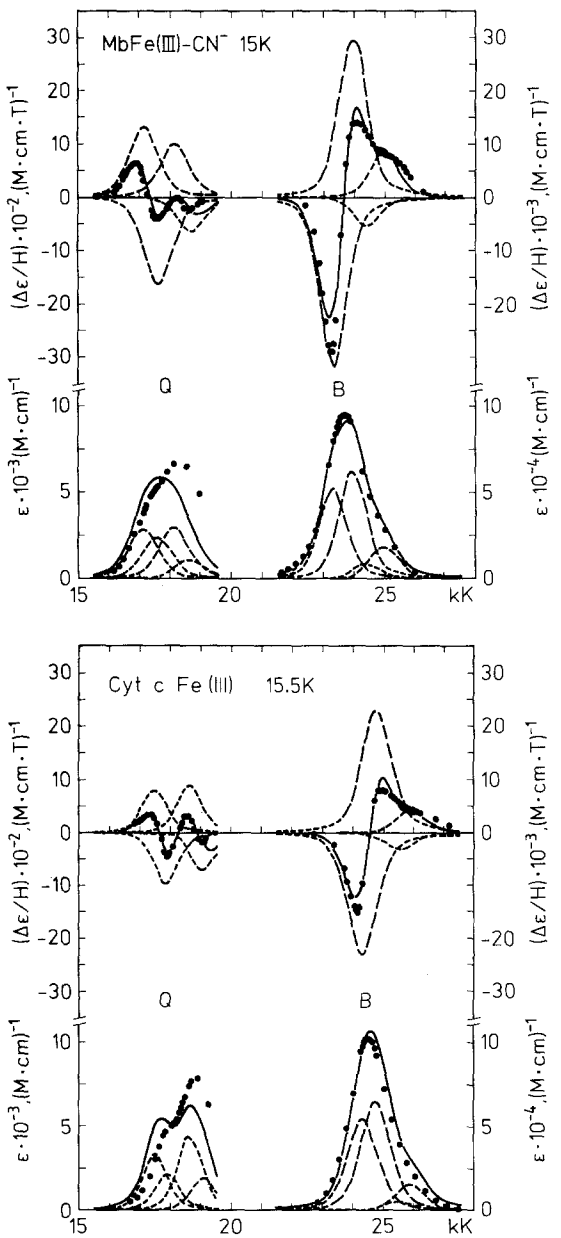


**Fig. 4.** The temperature-dependent MCD and the absorption compared with the experimental data. (a) MbCN (15 K); (b) cyt *c* (15.5 K). The corresponding values of parameters are listed in Table 3. The individual components are shown by dashed lines

about twice from low-temperature MCD reported by Springall et al. [4]. The MCD spectrum of ferricytochrome *c* in the Soret region at liquid helium temperatures has been reported previously [5]. The MCD spectra of horseradish peroxidase cyanide in the visible and near infrared regions at temperatures below 77 K are reported for the first time. The MCD spectra of these proteins at temperatures above 77 K have been published [1, 6–9] and agree well with those obtained in this paper.

## 3. Theory

The electronic structure of Fe(III)-ion in low-spin porphyrin complexes is accepted to be describable in terms of the model which has been proposed by Griffith to explain the EPR-spectra of these compounds [10]. According to this model, the spin-orbit coupling combined with tetragonal and rhombic distortions of the strong octahedral ligand field results in the splitting of $^2T_{2g}$-term into three Kramers doublets, any ($j$th) of which is conveniently described [11] by:

$$\begin{aligned} |K_j^+\rangle &= A_j|\xi\alpha\rangle - iB_j|\eta\alpha\rangle - C_j|\zeta\beta\rangle \\ |K_j^-\rangle &= -A_j|\xi\beta\rangle - iB_j|\eta\beta\rangle - C_j|\zeta\alpha\rangle \quad j = 1, 2, 3 \end{aligned} \tag{1}$$

where $A_j$, $B_j$ and $C_j$ are the real coefficients and $|\xi\alpha\rangle$, $|\eta\beta\rangle$ etc. are the wave functions of $t_{2g}$-hole, e.g.

$$|\xi\alpha\rangle \equiv |\zeta\bar{\zeta}\eta\bar{\eta}\bar{\xi}|.$$

Typical gap between the first and the second doublets has been evaluated to be about 1.5 $\lambda$ while that between second and third ones are about 3.5 $\lambda$ and even higher [11] (where $\lambda$ is the spin-orbit coupling constant which in the case of a free Fe(III)-ion has the value of 436 $cm^{-1}$). Moreover, the analysis of the EPR spectra [10, 11] shows that the first two doublets are mainly composed of strongly mixed $\xi$- and $\eta$-states, whereas the third doublet is in fact equivalent to $\zeta$-orbital. Since we search for the effects of $\langle L_z\rangle_d$ (which is non-zero due to $\xi$- and $\eta$-but not due to $\zeta$-orbital) we shall neglect here the contribution of $\zeta$-orbital and therefore we shall neglect high-energy third Kramers doublet. By this simplification the first two doublets may be rewritten as:

$$\begin{aligned} |K_1^+\rangle &= \sin\varphi|\xi\alpha\rangle + i\cos\varphi|\eta\alpha\rangle \\ |K_1^-\rangle &= -\sin\varphi|\xi\beta\rangle + i\cos\varphi|\eta\beta\rangle \\ |K_2^+\rangle &= -\cos\varphi|\xi\alpha\rangle + i\sin\varphi|\eta\alpha\rangle \\ |K_2^-\rangle &= \cos\varphi|\xi\beta\rangle + i\sin\varphi|\eta\beta\rangle \end{aligned} \tag{2}$$

where $\varphi$ is determined by

$$\operatorname{tg} 2\varphi = \frac{\lambda}{\langle\eta|V_{rh}|\eta\rangle - \langle\xi|V_{rh}|\xi\rangle} > 0 \tag{3}$$

**Table 1.** The values of $2\varphi$ (in degrees) calculated from the EPR data by different ways

| Compuund | $g_x$ | $g_y$ | $g_z$ | $\Delta E_{12}$ ($cm^{-1}$) | arcsin $\frac{\lambda}{\Delta E_{12}}$ | arccos $\frac{(g_x+g_y)}{4}$ | arcsin $\frac{(g_z-2)}{2}$ | arcsin $(2A_1B_1)$ | arccos $(A_1^2-B_1^2)$ | $-$arcsin $(2A_2B_2)$ | arccos $(A_2^2-B_2^2)$ | $2\varphi_{min}$ | $2\varphi_{max}$ |
|---|---|---|---|---|---|---|---|---|---|---|---|---|---|
| Cyt **c** | 1.24 | 2.24 | 3.06 [12] | 1.83 | 33.1 | 29.5 | 32.0 | 36.5 | 40.1 | 39.9 | 43.1 | 29.5 | 43.05 |
| HRP-$CN^-$ | 1.25 | 2.25 | 3.15 [13][a] | 1.79 | 34.0 | 29.0 | 35.1 | 37.5 | 40.9 | 40.7 | 43.4 | 29.0 | 43.4 |
| Mb$CN^-$ | 0.93 | 1.89 | 3.45 [14] | 1.45 | 43.7 | 45.2 | 46.5 | 47.7 | 51.7 | 51.6 | 52.5 | 43.7 | 52.5 |

[a] g-values were evaluated from diagram presented in [13], $A_j$, $B_j$ and $\Delta E_{12}$ were calculated in accordance with [11].

**Table 2.** Matrix of the $\pi - d$-interaction within the basis set defined by Eq. (5)

| $\phi_1^{\pm} = \begin{Bmatrix} B_{L1}^{+} \\ B_{\bar{R}1}^{-} \end{Bmatrix}$ | $\phi_2^{\pm} = \begin{Bmatrix} B_{R1}^{+} \\ B_{\bar{L}1}^{-} \end{Bmatrix}$ | $\phi_3^{\pm} = \begin{Bmatrix} B_{L2}^{+} \\ B_{\bar{R}2}^{-} \end{Bmatrix}$ | $\phi_4^{\pm} = \begin{Bmatrix} B_{R2}^{+} \\ B_{\bar{L}2}^{-} \end{Bmatrix}$ | $\phi_5^{\pm} = \begin{Bmatrix} Q_{L1}^{+} \\ Q_{\bar{R}1}^{-} \end{Bmatrix}$ | $\phi_6^{\pm} = \begin{Bmatrix} Q_{R1}^{+} \\ Q_{\bar{L}1}^{-} \end{Bmatrix}$ | $\phi_7^{\pm} = \begin{Bmatrix} Q_{L2}^{+} \\ Q_{\bar{R}2}^{-} \end{Bmatrix}$ | $\phi_8^{\pm} = \begin{Bmatrix} Q_{R2}^{+} \\ Q_{\bar{L}2}^{-} \end{Bmatrix}$ |
|---|---|---|---|---|---|---|---|
| $V_B - ((S - T\sin 2\theta)/2) \cdot \sin 2\varphi$ | $-D_2 \cos 2\varphi \cos 2\theta$ | $((S - T\sin 2\theta)/2) \cdot \cos 2\varphi$ | $(D_1 - D_2 \sin 2\varphi) \cdot \cos 2\theta$ | $T \sin 2\varphi \cos 2\theta$ | $D_2 \cos 2\varphi \sin 2\theta$ | $-T \cos 2\varphi \cos 2\theta$ | $-(D_1 - D_2 \sin 2\varphi) \cdot \sin 2\theta$ |
| | $V_B + ((S - T\sin 2\theta)/2) \cdot \sin 2\varphi$ | $-(D_1 + D_2 \sin 2\varphi) \cdot \cos 2\theta$ | $-((S - T\sin 2\theta)/2) \cdot \cos 2\varphi$ | $D_2 \cos 2\varphi \sin 2\theta$ | $-T \sin 2\varphi \cos 2\theta$ | $(D_1 + D_2 \sin 2\varphi) \cdot \sin 2\theta$ | $T \cos 2\varphi \cos 2\theta$ |
| | | $V_B + \Delta E_{12} + ((S - T\cos 2\theta)/2) \cdot \sin 2\varphi$ | $D_2 \cos 2\varphi \cos 2\theta$ | $-T \cos 2\varphi \cos 2\theta$ | $(D_1 + D_2 \sin 2\varphi) \cdot \sin 2\theta$ | $-T \sin 2\varphi \cos 2\theta$ | $-D_2 \cos 2\varphi \sin 2\theta$ |
| | | | $V_B + \Delta E_{12} - ((S - T\sin 2\theta)/2) \cdot \sin 2\varphi$ | $-(D_1 - D_2 \sin 2\varphi) \cdot \sin 2\theta$ | $T \cos 2\varphi \cos 2\theta$ | $-D_2 \cos 2\varphi \sin 2\theta$ | $T \sin 2\varphi \cos 2\theta$ |
| | | | | $V_Q - ((S + T\sin 2\theta)/2) \cdot \sin 2\varphi$ | $D_2 \cos 2\varphi \cos 2\theta$ | $((S + T\sin 2\theta)/2)\cos 2\varphi$ | $-(D_1 - D_2 \sin 2\varphi) \cdot \cos 2\theta$ |
| | | | | | $V_Q + ((S + T\sin 2\theta)/2) \cdot \sin 2\varphi$ | $(D_1 + D_2 \sin 2\varphi) \cdot \cos 2\theta$ | $-((S + T\sin 2\theta)/2) \cdot \cos 2\varphi$ |
| | | | | | | $V_Q + \Delta E_{12} + ((S + T\sin 2\theta)/2) \cdot \sin 2\varphi$ | $-D_2 \cos 2\varphi \cos 2\theta$ |
| | | | | | | | $V_Q + \Delta E_{12} - ((S + T\sin 2\theta)/2) \cdot \sin 2\varphi$ |

$$\Delta E_{12} = \frac{\lambda}{\sin 2\varphi}$$

$$T = \langle a_2 \xi | \eta a_1 \rangle$$

$$S = \frac{\langle e_x \xi | \eta e_y \rangle - \langle e_x \eta | \xi e_y \rangle}{2}$$

$$D_1 = \langle e_x \xi | e_y \eta \rangle - \frac{\langle e_x \xi | \eta e_y \rangle + \langle e_x \eta | \xi e_y \rangle}{4}$$

$$D_2 = \frac{\langle e_x \eta | e_x \eta \rangle - \langle e_x \xi | e_x \xi \rangle}{2} - \frac{\langle e_x \eta | \eta e_x \rangle - \langle e_x \xi | \xi e_x \rangle}{4}$$

$$\langle ik | jl \rangle = \int i^*(1) k^*(2) \frac{e^2}{r_{12}} j(1) 1(2) d\tau_{12}$$

and

$$|\xi\alpha\rangle = -|\eta\bar{\eta}\xi| \qquad |\xi\beta\rangle = -|\eta\bar{\eta}\bar{\xi}|$$
$$|\eta\alpha\rangle = |\xi\bar{\xi}\eta| \qquad |\eta\beta\rangle = |\xi\bar{\xi}\bar{\eta}|. \tag{3a}$$

From this approximation it follows that $g_x = g_y = 2\cos 2\varphi$ and $g_z = 2(1+\sin 2\varphi)$. In reality the in-plane anisotropy ($g_x \neq g_y$) is clearly observed (see Table 1). Thus the $\varphi$-value of Eqs. (2), (3) which we use further as a fixed parameter could not be unambiguously obtained from the EPR-data. For this reason we choose $\varphi$ from the certain range of $\varphi$-values given in Table 1.

To describe the electronic states of the porphyrin ring we use the so-called "four-orbital model" proposed by Gouterman [15]. So the overall ferriheme (Fe(III) + porphyrin) electronic states are given by

a. unexcited in-porphyrin states:

$$|G_1^{\pm}\rangle = \{a_{1u}^2 a_{2u}^2 K_1^{\pm}\}$$
$$|G_2^{\pm}\rangle = \{a_{1u}^2 a_{2u}^2 K_2^{\pm}\} \tag{4}$$

b. $\pi - \pi^*$-excited states:

$$|B_{Lj}^{\pm}\rangle = \{B_L K_j^{\pm}\} \qquad |B_{Rj}^{\pm}\rangle = \{B_R K_j^{\pm}\}$$
$$|Q_{Lj}^{\pm}\rangle = \{Q_L K_j^{\pm}\} \qquad |Q_{Rj}^{\pm}\rangle = \{Q_R K_j^{\pm}\}. \tag{5}$$

The excited porphyrin states are described here in terms of circular components $|L\rangle = (|X\rangle + i|Y\rangle)/\sqrt{2}$ and $|R\rangle = (|X\rangle - i|Y\rangle)/\sqrt{2}$ where $|X\rangle$ and $|Y\rangle$ represent the corresponding Gouterman functions [15]:

$$B_x = \sin\theta\{a_{1u}e_{gy}\} + \cos\theta\{a_{2u}e_{gx}\}$$
$$B_y = -\sin\theta\{a_{1u}e_{gx}\} + \cos\theta\{a_{2u}e_{gy}\}$$
$$Q_x = \cos\theta\{a_{1u}e_{gy}\} - \sin\theta\{a_{2u}e_{gx}\}$$
$$Q_y = -\cos\theta\{a_{1u}e_{gx}\} - \sin\theta\{a_{2u}e_{gy}\}. \tag{6}$$

In Eqs. (4), (6) $a_{1u}$ and $a_{2u}$ are the top filled quasidegenerate porphyrin orbitals and $e_g$ is the lowest-lying empty orbital. The $\{a_{1u}e_{gy}\}$ etc. represent the excited singlet configuration after the corresponding transition, and $\theta$ is defined by [15]:

$$\operatorname{tg} 2\theta = \frac{4\langle a_{2u}e_{gy}|e^2/r_{12}|e_{gx}a_{1u}\rangle}{E(\{a_{2u}e_g\}) - E(\{a_{1u}e_g\})}. \tag{7}$$

It is not difficult to see that 16 states given by Eq. (5) form 8 Kramers doublets: $\{B_{L1}^{+}; B_{R1}^{-}\}$; $\{B_{R1}^{+}; B_{L1}^{-}\}$ etc., therefore the matrix of the $T$-even operator of the Coulomb interaction, $\sum_{i<j} e^2/r_{ij}$, factors into two identical $8\times 8$-matrices (Table 2). The diagonalization results in eight new Kramers doublets:

$$\psi_j^{\pm} = \sum_{i=1}^{8} a_{ij}\Phi_i^{\pm} \quad (j = 1, 2, \ldots 8) \tag{8}$$

where wavefunctions $\Phi_i^{\pm}$ denote the basis doublets in order of their appearance in Table 2 (e.g. $\Phi_1^+ = B_{L1}^+$, $\Phi_1^- = B_{R1}^-$ etc.). The wavefunctions $\psi_j^{\pm}$ could be used to calculate the MCD and the absorption spectra.

To simplify the computer procedure, we calculate only the $C$-type effects of the MCD spectra which are to be fitted to the temperature dependent contribution to MCD ($\Delta\varepsilon_M^C$). When $\Delta\varepsilon_M^C$ depends linearly on 1/T it could be easily extracted from the experimental MCD curves recorded at two different temperatures ($\Delta\varepsilon_M(T_1)$, $\Delta\varepsilon_M(T_2)$) [16]:

$$\Delta\varepsilon_M^C = \frac{1}{T}\frac{T_1 T_2}{T_2 - T_1}[\Delta\varepsilon_M(T_1) - \Delta\varepsilon_M(T_2)].$$

Furthermore, the absorption spectra were compared with those calculated using the wavefunctions of Eq. (8).

To calculate the theoretical spectral curves we have used Eqs. (7) and (10) from ref. [17] which operate with random oriented molecules, so that the spectra of interest are given by

$$\begin{aligned} \Delta\varepsilon_M^C &= -2\gamma\frac{H_z}{kT}\sum_{j=1}^{8} C_j f(\nu, \nu_j, \Gamma_j) \\ \varepsilon &= \gamma\sum_{j=1}^{8} D_j f(\nu, \nu_j, \Gamma_j) \end{aligned} \tag{9}$$

here $\gamma$ lumps together a number of constants, $f(\nu, \nu_j, \Gamma_j)$ defines the bandshape with half-width $\Gamma_j$ occurred at frequency $\nu_j = E_j/h$ (where $E_j$ is the $j$th eigenvalue of matrix represented by Table 2). In our case the parameters $C_j$ and $D_j$ related with transition to the excited state $\psi_j^{\pm}$ are given by

$$\begin{aligned} C_j = \tfrac{1}{4}\{&[|\langle G_1^+|m_+|\psi_j^+\rangle|^2 - |\langle G_1^+|m_-|\psi_j^+\rangle|^2]\langle G_1^+|\mu_z|G_1^+\rangle \\ &+[|\langle G_1^-|m_+|\psi_j^-\rangle|^2 - |\langle G_1^-|m_-|\psi_j^-\rangle|^2]\langle G_1^-|\mu_z|G_1^-\rangle\} \end{aligned} \tag{10}$$

$$\begin{aligned} D_j = \tfrac{1}{2}[&|\langle G_1^+|m_+|\psi_j^+\rangle|^2 + |\langle G_1^+|m_-|\psi_j^+\rangle|^2 \\ &+|\langle G_1^-|m_+|\psi_j^-\rangle|^2 + |\langle G_1^-|m_-|\psi_j^-\rangle|^2] \end{aligned} \tag{11}$$

where $m_{\pm} = (m_x \pm i m_y)/\sqrt{2}$ are circular components of the electric dipole operator, $\mu_z = -\beta(l_z + 2s_z)$ ($\beta > 0$ is the electronic Bohr magneton) and the wavefunctions of the ground ($G_1^{\pm}$) and excited ($\psi_j^{\pm}$) states are given by Eqs. (4) and (8), respectively. (The population of the second Kramers doublet $G_2^{\pm}$ is negligibly small, even at room temperature since its energy is of the order of $10^3$ cm$^{-1}$ [11]).

Taking into account that

$$-\langle G_1^+|\mu_z|G_1^+\rangle = \langle G_1^-|\mu_z|G_1^-\rangle = \frac{\beta g_z}{2}$$

and adopting the Gouterman approximation [15] that $\langle a_{1u}|m_x|e_{gy}\rangle = \langle a_{2u}|m_x|e_{gx}\rangle$

and therefore

$$\frac{\langle G^{\pm}|m_+|Q_R^{\pm}\rangle}{\langle G^{\pm}|m_+|B_R^{\pm}\rangle}=\frac{\langle G^{\pm}|m_-|Q_L^{\pm}\rangle}{\langle G^{\pm}|m_-|B_L^{\pm}\rangle}=\frac{\cos\theta-\sin\theta}{\cos\theta+\sin\theta}=\varkappa \tag{12}$$

we obtain

$$C_j=\frac{\beta g_z}{4}[(a_{1j}+\varkappa a_{5j})^2-(a_{2j}+\varkappa a_{6j})^2]|\langle G_1^{\pm}|m_+|B_R^{\pm}\rangle|^2 \tag{13}$$

$$D_j=[(a_{1j}+\varkappa a_{5j})^2+(a_{2j}+\varkappa a_{6j})^2]|\langle G_1^{\pm}|m_+|B_R^{\pm}\rangle|^2. \tag{14}$$

Finally, substituting Eqs. (13) and (14) into Eq. (9) we obtain the expressions for the theoretical MCD (temperature dependent) and absorption spectra:

$$\Delta\varepsilon_M^C(\nu, T, H)=-\gamma\frac{\beta g_z H}{2kT}|\langle G^+|m_+|B_R^+\rangle|^2\sum_{j=1}^{8}[(a_{1j}+\varkappa a_{5j})^2 -(a_{2j}+\varkappa a_{6j})^2]f(\nu, \nu_j, \Gamma_j) \tag{15}$$

$$\varepsilon(\nu)=\gamma|\langle G_1^+|m_+|B_R^+\rangle|^2\sum_{j=1}^{8}[(a_{1j}+\varkappa a_{5j})^2 +(a_{2j}+\varkappa a_{6j})^2]f(\nu, \nu_j, \Gamma_j). \tag{16}$$

## 4. Fit Procedure and Results

The least squares fit was carried out simultaneously to the MCD and absorption data. Taking into account that the short-wavelength part of the $Q$-region might be partially descended from the vibronic satellites ($Q_{01}$- or $\beta$-band), the experimental points were more widely spaced within this region as compared to the longwavelength part. By doing so we attempted to fit in the first place the pure electronic moiety of the $Q$-band. At the same time we did not completely ignore the "blue" part of the $Q$-band which was assumed to be mainly formed by two-photon electronic transitions (see below).

The computer minimized the following values:

$$Z=w_{B,\mathrm{MCD}}\sum_{i\in B}(\Delta\varepsilon_{\mathrm{Mi}}^{\mathrm{th}}-\Delta\varepsilon_{\mathrm{Mi}}^{\mathrm{ex}})^2$$

$$+w_{B,\mathrm{Abn}}\sum_{i\in B}(\varepsilon_i^{\mathrm{th}}-\varepsilon_i^{\mathrm{ex}})^2$$

$$+w_{Q,\mathrm{Abn}}\sum_{i\in Q}(\Delta\varepsilon_{\mathrm{Mi}}^{\mathrm{th}}-\Delta\varepsilon_{\mathrm{Mi}}^{\mathrm{ex}})^2$$

$$+w_{Q,\mathrm{Abn}}\sum_{i\in Q}(\varepsilon_i^{\mathrm{th}}-\varepsilon_i^{\mathrm{ex}})^2$$

where $\Delta\varepsilon_{\mathrm{Mi}}^{\mathrm{th}}$ and $\varepsilon_i^{\mathrm{th}}$ are the theoretical values calculated with Eqs. (15) and (16), respectively, at the same frequencies where the experimental values $\Delta\varepsilon_{\mathrm{Mi}}^{\mathrm{ex}}$

and $\varepsilon_i^{ex}$ were plotted. The weights, $w$, could be varied arbitrarily, but commonly they were chosen to satisfy the following relationships:

$$w_{B,\mathrm{MCD}} \sum_{i\in B} (\Delta\varepsilon_{\mathrm{Mi}}^{ex})^2 = w_{B,\mathrm{Abn}} \sum_{i\in B} (\varepsilon_i^{ex})^2$$

$$= w_{Q,\mathrm{MCD}} \sum_{i\in Q} (\Delta\varepsilon_{\mathrm{Mi}}^{ex})^2 \equiv A$$

$$0 \leqslant w_Q \sum_{i\in Q} (\varepsilon_i^{ex})^2 \leqslant A/2.$$

In other words, we tried to give no preference to any of the three experimental spectra (MCD in both $B$- and $Q$-regions and absorption in $B$-region). At the same time the theoretical absorption in the $Q$-region was sometimes simply displayed in accordance to the parameters obtained by the fitting to these three spectra. Such an approach seemed to be justified by the fact that the vibronic components which were not involved in our model contribute essentially to the visible absorption spectra.

The weights, once chosen at the start of any fitting, remained constant as well as the values of spin-orbit coupling ($\lambda = 436\ \mathrm{cm}^{-1}$), Fe-rhombisity parameter $\varphi$ (see Table 1) and the fraction of the Lorentz function ($\alpha$) in the band shape, $f(\nu, \nu_j, \Gamma_j)$ which were chosen as the linear combination of Lorentz ($f_L$) and Gauss ($f_G$) shapes:

$$f(\nu, \nu_0, \Gamma) = \alpha f_L + (1-\alpha) f_G$$

where

$$f_L = \frac{\Gamma\nu^3}{(\nu_0^2 - \nu^2)^2 + (\Gamma\nu)^2};$$

$$f_G = \frac{2\nu}{\Gamma} \exp\{-2(\ln 2)^{-1/2}[(\nu-\nu_0)/\Gamma]^2\}.$$

The best results were obtained with $\alpha = 0.62$.

The nine adjustable parameters $V_B$, $V_G$, $S$, $T$, $D_1$, $D_2$, $\theta$, $\Gamma_B$ and $\Gamma_Q$ were determined (see Table 2). The two latters, $\Gamma_B$ and $\Gamma_Q$, were chosen to be equal for each of four $B$- and $Q$-components, respectively ($\Gamma_1 = \ldots = \Gamma_4 = \Gamma_B$; $\Gamma_5 = \ldots = \Gamma_8 = \Gamma_Q$). The computer diagonalized the matrix given by Table 2 at any given input parameter set and then simulated the theoretical spectra using Eqs. (15) and (16). The amplitude factor $|\langle G|m_+|B_R\rangle|^2$ was fitted at every trial step. A somewhat modified method of Rosenbrock was used [18].

The results of the least squares procedure are summarized in Table 3. Figure 4 shows the results of the fitting for MbCN (a) and cyt *c*, (b) respectively. They also contain the separate components of summarized theoretical curves.

The fitting procedure was preceded by two stages. At the first one, only the spectra in the $B$-region were fitted. It requires not 9 but only 6 adjustable

**Table 3.** Parameters obtained by fitting procedure

| Compound | $V_Q$ | $V_B$ | $\Gamma_Q$ | $\Gamma_B$ | $S$ | $T$ | $D_1$ | $D_2$ | $2\theta$ | $2\varphi$[a] |
|---|---|---|---|---|---|---|---|---|---|---|
| | | | | ($cm^{-1}$) | | | | | (degrees) | |
| Cyt *c* | 18 245 | 24 292 | 969 | 1154 | 87 | −383 | 1660 | 157 | 72.8 | 31.0 |
| HRP-$CN^-$ | 17 811 | 23 599 | 810 | 872 | 177 | −524 | 1498 | 226 | 72.2 | 38.0 |
| MbCN | 17 942 | 23 453 | 1134 | 1050 | 94 | −456 | 1541 | 205 | 71.6 | 46.0 |

[a] See Table 1; $\lambda = 436\ cm^{-1}$; $\alpha = 0.62$.

parameters, namely $V_B$; $D_1$; $D_2$; $\theta$; $\Gamma_B$ and $(st) = S - T \sin 2\theta$ (see Table 2). Several final parameter sets were then used as fixed input ones for the second stage.

From the beginning, the second stage involved the fitting in neglecting the $B-Q-(\pi\text{-}d)$-mixing, i.e. the $8\times8$-matrix of $\pi-d$-interaction was represented as block-diagonal one $B(4\times4)\times Q(4\times4)$. However neither of the sets of $T$, $V_Q$ and $\Gamma_Q$ which could satisfactorily describe the visible spectra was found. At last the diagonalization of the full $8\times8$ matrix was made and the three parameters ($T$, $\nu_Q$ and $\Gamma_Q$) were permitted to vary. Just at this stage, the selection of the first stage sets was carried out. The satisfactory results have been obtained only for one of these input sets (except the simultaneous change of signs of number of $\pi-d$-parameters induced by the alternative choice of the wavefunction phase). The nine parameters thus obtained were used to determine the ultimate parameter set by the simultaneous variation of all nine adjustable values.

## 5. Discussion

Thus both the low-temperature MCD and the absorption of low-spin ferriheme compounds in the visible $Q$-and near UV $B$-bands seem to be understood in some details in terms of the $\pi-d$-interaction scheme.

The $\pi-d$-parameters $D_1$, $D_2$ and $S$ could be best comprehended by considering the symmetrized excited configurations. In the case of $a_{1u}\rightarrow e_g$-transition there are four symmetrized iron-porphyrin ($E_g\times E_u$) configurations (spin effects are ommitted):

$$|1A_{1u}\rangle \sim \{a_{1u}e_{gx}\eta\} + \{a_{1u}e_{gy}\xi\}$$

$$|1A_{2u}\rangle \sim \{a_{1u}e_{gx}\xi\} - \{a_{1u}e_{gy}\eta\}$$

$$|1B_{1u}\rangle \sim \{a_{1u}e_{gx}\eta\} - \{a_{1u}e_{gy}\xi\}$$

$$|1B_{2u}\rangle \sim \{a_{1u}e_{gx}\xi\} + \{a_{1u}e_{gy}\eta\}.$$

In the presence of the Coulomb repulsion between $\pi$- and $d$-electrons these configurations will have different energies. The corresponding energy levels and the gaps between them expressed in terms of $D_1$, $D_2$ and $S$ are shown in Fig. 5. The similar diagram could be constructed for the excited configurations resulted from $a_{2u}\rightarrow e_g$-transition.

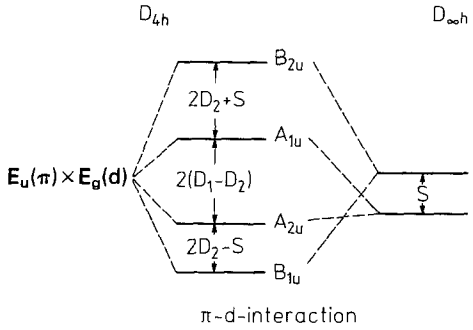


**Fig. 5.** The $\pi-d$-term scheme for $a_{1u}(\pi)\rightarrow e_g(\pi^*)$-transition

The mixing of these symmetrized states which occurs due to configuration $\pi$-$\pi$-interaction [15] and its $\pi-d$-analogue (T) as well as due to the spin-orbit coupling and rhombicity on the Fe-ion results in the new states given by Eq. 8. It should be noted here that the rhombic axes of the ligand field were assumed to coincide with $N-N$-directions of porphyrin ring. It may be shown that the rotation of the rhombic field axes about the heme normal through an angle 45° (the replacement of the $B_1$-symmetry rhombicity by $B_2$-symmetry one) would result in the general substitution of the parameter $D_1$ by $D_2$ and vice versa. When rhombic axes are rotated through an arbitrary angle $\alpha$ with respect to porphyrin $x$-, $y$-axes, two additional parameters should be included, namely the irreducible matrix element of the $B_2$-rhombicity operator and the angle $\alpha$ itself. However we believed this would exceed the accuracy of the model. Our choice of the rhombicity symmetry was based on the Mössbauer data by Rhynard et al. who evaluated $\alpha$ to be as small as 8° for MbCN [19].

In paper [1] we did not take into consideration the parameters $D_1$ and $D_2$ and hence we dealt with two degenerate pairs $A_1 \div A_2$ and $B_1 \div B_2$ (Fig. 5, right). Moreover we did not include neither the second Kramers doublet of Fe(III)-ion, nor the $\pi-d$-mixing between $B$- and $Q$-states. In other words, instead of $8\times 8$-matrix of $\pi-d$-interaction we confined ourselves to the two $2\times 2$-matrices which could be diagonalized by the choice of the $B_{L1}$, $B_{R1}$- and $Q_{L1}$, $Q_{R1}$-bases, respectively. This case is illustrated in Fig. 6a. (The different signs of the MCD in $B$- and $Q$-bands arise because of the $\pi-d$-splitting in the $B$-band, $\Delta_B^{\pi-d} = S - T \sin 2\theta$, is positive at a given choice of parameters, whereas that in the $Q$-band, $\Delta_Q^{\pi-d} = S + T \sin 2\theta$, is negative. Generally, the different signs will be observed when $|S| < |T \sin 2\theta|$.)

If within the same basis sets the real symmetry of the system is now taken into accoutn ($2\theta \neq 90°$, $2\varphi \neq 90°$, $D_2 \neq 0$) the $B$- and $Q$-$2\times 2$-matrices will be no longer diagonal ones. (The matrix elements (1,2) and (5,6) of $8\times 8$-matrix become nonzero.) This results in i) the mixing of the basis states and ii) the enhancement of the $\pi-d$-splitting between them.

Because of i) an amplitude of each individual MCD component will diminish. (In the limits of a complete $L-R$-mixing apparently $\varepsilon_L - \varepsilon_R = 0$). Because of ii) the MCD components of different signs will annihilate each other to a lower

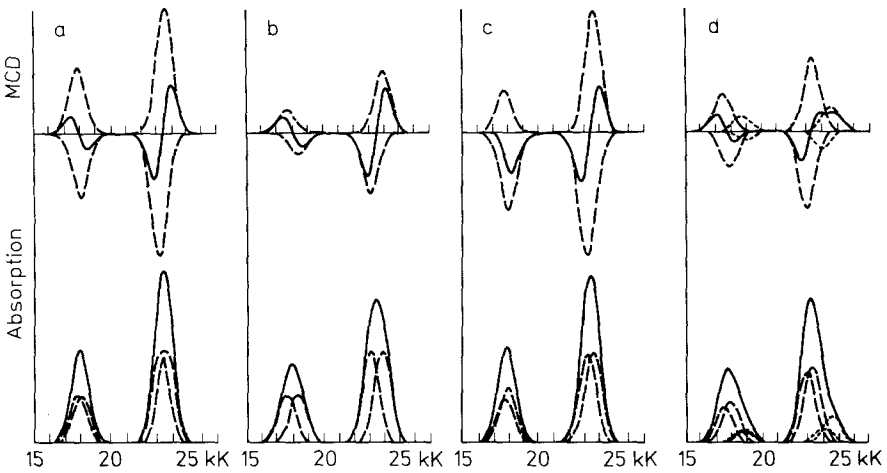


**Fig. 6.** The temperature-dependent MCD and absorption simulated for the various approximations of the model. The individual components $f_i = (\nu/\nu_{oi}) \exp[-(\nu-\nu_{oi})^2/\Gamma^2]$ ($\Gamma = 800\ cm^{-1}$) are shown by dashed lines. $Q$-bands are enlarged by 20 times. $S = 94\ cm^{-1}$, $T = -456\ cm^{-1}$, $V_Q = 17942\ cm^{-1}$, $V_B = 24453\ cm^{-1}$, $2\theta = 71.6°$, $2\varphi = 46°$ (see the third line in Table 3). (a) The ground Fe(III)-ion Kramers doublet only. $B-Q$-mixing is absent, $D_2 = 0$; (b) the same as (a), but $D_2 = 1541\ cm^{-1}$; (c) the same as (a) but $B-Q$-mixing is taken into account, $D_2 = 205\ cm^{-1}$; (d) the first excited Fe(III)-ion doublet is taken into account, but $B-Q$-mixing is absent, $D_1 = 1541\ cm^{-1}$, $D_2 = 205\ cm^{-1}$

extent as compared with the previous $D_{\infty h}$-case. Hence the amplitude of the summarized MCD signal ought to increase. It is not difficult to show that provided $\Delta^{\pi-d} \lesssim \Gamma$ the simultaneous effect of both i) and ii) will compensate each other and the MCD amplitude will remain equal to that observed in a previous case (cf. Figs. 6a and b). On the contrary in the absorption the $L-R$-mixing does not reduce the amplitude of any of individual components. However the increase of $\Delta^{\pi-d}$ results both in some broadening and decrease of the amplitude of the summarized absorption bands (Fig. 6b, bottom). For the further development of the model the $\pi-d$-mixing of $B$- and $Q$-bands is to be considered. Although any of $B-Q$-mixing matrix elements are surely small as compared with the energy difference $V_B - V_Q \simeq 1$ eV the effect of this mixing is expected to be crucial for the $Q$-band. It follows from the fact that the intensity of a porphyrin $Q$-band is known to be about $10^2$ times less than that of $B$-band. Thus even small intensity borrowing from the strong $B$-band owing to $\pi-d$-mixing could in principle affect markedly on the quasiforbidden $Q$-band.

To illustrate such a situation let us consider the particular case when the rhombicity on the Fe(III)-ion is absent ($2\varphi = 90°$) and the second Fe(III)-ion doublet $K_2^{\pm}$ is neglected. Then in the first order (see Matrix given by Table 2);

$$\Phi_5^{\pm(1)} = \Phi_5^{\pm} - \kappa\Phi_1^{\pm}$$

$$\Phi_6^{\pm(1)} = \Phi_6^{\pm} + \kappa\Phi_2^{\pm}$$

where $\kappa = T\cos 2\theta/(V_B - V_Q)$ reflects the degree of mixing between $B$- and $Q$-component of the same circular polarization. Using now Eq. (15) one can

evaluate the ratio of the "new" MCD components within the $Q$-band as $[(\varkappa - \kappa)/(\varkappa + \kappa)]^2$ which is generally not equal to unity. This asymmetry of the MCD signal in the $Q$-band may be fairly significant so that the summarized MCD would look like a single $C$-type effect, but the extremum position of this absorption-like MCD band will not generally coincide with that of the absorption band. At the same time the strong $B$-band remains in fact invariable (see Fig. 6c).

The importance of including the excited Kramers doublet $K_2^{\pm}$ follows just from comparing its typical energy ($\simeq 10^3$ cm$^{-1}$ [11]) with the value of $\pi - d$-splitting which for the first time has been evaluated from the MCD data as great as $5 \cdot 10^2$ cm$^{-1}$ [8]. Because of the same order of these two values one could expect an efficient $\pi - d$-mixing between allowed $G_1 \rightarrow Q_1, B_1$-transitions and forbidden two-photon $G_1 \rightarrow Q_2, B_2$-transitions. As a result both $B$- and $Q$-bands acquire the four-component structure. The spectrum of this band is shown in Fig. 6d, where the effects of $B - Q$-mixing are ignored.

The diagonalization of full $8 \times 8$-matrix results in theoretical spectra described by Eqs. (15) and (16). The components of eigenvectors $a_{ij}$ reflect as usual the weights of the basis wavefunctions $|i\rangle$ in the new states $|j\rangle$. Since before $\pi - d$-interaction the allowed transitions were $G_1 \rightarrow \Phi_1, \Phi_2, \Phi_5, \Phi_6$ the new intensities are determined by the four sets of the following values $a_{1j}$, $a_{2j}$, $\varkappa a_{5j}$ and $\varkappa a_{6j}$. Thus the value $(a_{1j} + \varkappa_{5j})^2$ reflects the absorption of the left polarized light for any given transition $G_1 \rightarrow \psi_j$ whereas $(a_{2j} + \varkappa a_{6j})^2$ reflects that of right polarized light. The difference between these values is proportional to the (magnetic) circular dichroism, and the sum determines the absorption. It is seen from Eqs. (15), (16) that the MCD-to-absorption ratio is no longer equal to $\beta g_z H/2kT$ as it is expected in the absence of the $\pi - d$-mixing between basis functions $\Phi_i^{\pm}$.

This point is especially interesting in the case of $Q$-band where $|\varkappa a_{5,6j}| \simeq |a_{1,2j}|$, and hence the effects of $\pi - d$-borrowing from $B$-band intensity may be quite marked. That is why the $Q$-band may be very sensitive to the change of the $\pi - d$-parameters which in turn depend on both $\pi$- and $d$-electronic structures. This sensitivity is expected to reveal in the MCD rather than in absorption because of differential character of the former.

The similar explanation of the striking differences observed between low-temperature $Q$-band MCD of deoxyhemoglobin and deoxymyoglobin and their photodissociated forms [2] is now in progress. We hope that such an approach will be successful in understanding of the ground-state structure in high-spin ferrous heme which stays yet unknown despite intense studies by Mössbauer spectroscopy and magnetic susceptibility measurements.

It would be interesting to compare the values of the $\pi - d$-parameters from Table 3 with those calculated quantumchemically by Seno et al. in their attempt to interpret the low-temperature MCD of high-spin ferrous myoglobin [20]. Unfortunately the authors have evaluated only two $\pi - d$-integrals namely (in accepted here notations) $\langle e_x\xi|\eta e_y\rangle = 700$ cm$^{-1}$ and $\langle e_x\xi|e_y\eta\rangle = 70$ cm$^{-1}$. Thus only $\pi - d$-value comparable with that of Seno et al. is the combination $|2D_1 - S| = |2\langle e_x\xi|e_y\eta\rangle - \langle e_x\xi|\eta e_y\rangle|$. Using the values listed in Table 3 this combination is

approximately equal to 3000 $cm^{-1}$ (or 300 $cm^{-1}$ with the parameter $D_2$ taken instead of $D_1$). On the other hand, according to Seno et al. this value is equal to 560 $cm^{-1}$, i.e. lies between our values.

In conclusion we should like to note two experimental observations which are not described in the framework of our theoretical model.

First, at low temperatures at least two new MCD bands appear between *B*- and *Q*-bands (Fig. 2). A possible cause of these extra bands exists in the third iron Kramers doublet (the transitions to $\{QK_3^{\pm}\}$-states). If this assumption is valid, the similar blue satellites are to be expected for *B*-band. However we didn't take into consideration the third iron doublet for the reasons discussed above.

Second, we have found that the 695 nm MCD band of ferricytochrome *c* is proportional to 1/T in the temperature used (Fig. 3). Eaton and Hochstrasser [21] assigned from the polarization measurements 695 nm band to the $a_{2u}(\pi) \rightharpoonup a_{1g}(d_z)^2$ charge transfer transition. This conclusion appeared to be consistent with the room-temperature MCD results of Sutherland and Klein [7]. However the straightforward substitution of these transitions in the expressions for MCD would result in zero *C*-type effects. We believe this discrepancy might be overcome by involving a borrowing mechanism from $\pi-\pi^*$-bands similar to that considered by Seno et al. [20] in their analysis of near IR MCD of deoxymyoglobin.

## 6. Conclusions

To explain a number of pecularities observed in the low-temperature MCD of low-spin ferriheme compounds, we propose an extended $\pi-d$-interaction model. This model includes the first excited ("second") iron Kramers doublet. For each $\pi-\pi^*$-transition the two possible states of Fe(III)-ion are considered. The two-quantum excited states appear to mix effectively with the allowed ones by $\pi-d$-interaction. Generally, this results in an asymmetry of MCD $\pi-\pi^*$-bands. Apart from the mixing of different states coupled with the same $\pi-\pi^*$-transition the $\pi-d$-interaction is able to mix the various (one- and two-photon) components of $B(\pi-\pi^*)$- and $Q(\pi-\pi^*)$-bands of ferriheme. This $B-Q$-mixing is of special importance for the *Q*-band because of its quasiforbidden character. Moreover, within the $B-Q$-mixing approach it becomes possible to explain the unusual mutual positions of MCD and absorption *Q*-bands and to ascribe the significant fraction of the absorption of the diffuse *Q*-band to the pure electronic effects without involving vibronic interactions. Four $\pi-d$-parameters are evaluated for three different species experimentally studied.

The proposed theoretical ideas seem to be fruitful for the further investigations of paramagnetic heme compounds.

*Acknowledgements.* We wish to acknowledge Prof. M. V. Volkenstein for his encouragement.

## References

1. Mineyev, A. P., Sharonov, Yu, A.: Theoret. Chim. Acta (Berl.) **49**, 295 (1978)
2. Sharonov, Yu. A., Sharonova, N. A., Figlovsky, V. A., Grigorjev, V. A.: Biochim. Biophys. Acta **709**, 332 (1982)
3. Vickery, L., Nozawa, T., Sauer, K.: J. Am. Chem. Soc. **98**, 343 (1976)
4. Springall, J., Stillman, M. J., Thomson, A. J.: Biochim. Biophys. Acta **453**, 494 (1976)
5. Thomson, A. J., Johnson, M. K.: Biochem. J. **191**, 411 (1980)
6. Nozawa, T., Kobayashi, N., Hatano, M.: Biochim. Biophys. Acta **427**, 652 (2976)
7. Sutherland, J. C., Klein, M. P.: J. Chem. Phys. **57**, 76 (1972)
8. Livshitz, M. A., Arutyunyan, A. M., Sharonov, Yu. A.: J. Chem. Phys. **64**, 1276 (1976)
9. Vickery, L., Nozawa, T., Sauer, K.: J. Am. Chem. Soc. **98**, 351 (1976)
10. Griffith, J. S.: Nature **180**, 30 (1957)
11. Taylor, C. P. S.: Biochim. Biophys. Acta **491**, 137 (1977)
12. Mailer, C., Taylor, C. P. S.: Can. J. Biochem. **50**, 1048 (1972)
13. Blumberg, W. E., Peisach, J.: in Probes of structure and function of macromolecules and membranes, B. Chance, T. Yonetani and A. S. Mildvan, Eds, Vol. 2, p. 215. New York; Academic Press 1971
14. Hori, H.: Biochim. Biophys. Acta **251**, 227 (1971)
15. Gouterman, M.: J. Chem. Phys. **30**, 1139 (1959)
16. Sharonov, Yu. A., Mineyev, A. P., Livshitz, M. A., Sharonova, N. A., Zhurkin, V. B., Lysov, Yu. P.: Biophys. Struct. Mechanism **4**, 139 (1978)
17. Stephens, P. J.: Ann. Rev. Phys. Chem. **25**, 201 (1974)
18. Rosenbrock, H. H.: Computer J. **3**, 175 (1960)
19. Rhynard, D., Lang, G., Spartalian, K., Yonetani, T.: J. Chem. Phys. **71**, 3715 (1979)
20. Seno, Y., Kameda, N., Otsuka, J.: J. Chem. Phys. **72**, 6059 (1980)
21. Eaton, W. A., Hochstrasser, R. M.: J. Chem. Phys. **46**, 2533 (1967)

Received November 11, 1982/February 21, 1983